Structural and Multidisciplinary Optimization (2024) 67:33
https://doi.org/10.1007/s00158-024-03759-1

RESEARCH PAPER

Large-scale topology optimization for dynamic problems using a repetitive substructuring approach

Hyeong Seok Koh[1] · **Gil Ho Yoon**[1]

Received: 20 April 2023 / Revised: 10 November 2023 / Accepted: 31 January 2024

Abstract
This paper proposes a novel technique for large-scale *partial* topology optimization of dynamic engineering structures by utilizing substructuring techniques and repetitive geometry. *Partial* topology optimization refers to a design domain that only covers a part of the overall analysis domain, involving multiple subdomains. While large-scale topology optimization techniques for static systems have made significant progress over the past few decades, techniques for dynamic systems, especially those in the frequency domain, face challenges due to matrix conditioning and preconditioning problems for iterative solvers. To overcome these challenges, this paper dramatically reduces the system's size through a substructuring approach to utilize a direct linear solver. Using a bottom-up style substructuring technique, all the finite element (FE) models are defined separately and in parallel, and the FE models in the non-design domains are approximated using the idea of repetitive geometry with the same discretization, while the models in the design remain intact. This approach eliminates conventional model reduction-based topology optimization problems, such as eigen-analysis and recovery processes for every iteration. The proposed technique enables a more realistic and feasible design of large-scale engineering structures in the frequency domain. Several numerical examples verify the performance of the presented method for partial topology optimization of large-scale models. Overall, this paper provides a novel and efficient approach to partial topology optimization for dynamic engineering structures, opening up new possibilities for realistic and feasible design in the frequency domain.

Keywords Substructuring method · Partial topology optimization · Large-scale topology optimization · Dynamic topology optimization · Multi-domain design

1 Introduction

Topology optimization (TO) has gained popularity in many engineering disciplines since Bendsøe and Kikuchi's groundbreaking study (Bendsøe and Kikuchi 1988). The fundamental idea of TO is to interpolate the material properties of each element from nonstructural domains to structural domains by introducing the concept of structural density, which varies from 0 (very small number) to 1. This approach provides various advantages, including a flexible parametrization of the design space, ease of integration with existing computational codes in various applications, and efficient sensitivity analysis. However, several challenges prevent TO from becoming a mainstream design method in actual industry fields. One of the main challenges is the computational complexity associated with solving the governing equations of the system, typically the partial differential equations, for optimization. The TO procedure requires repeatedly solving discretized PDEs, and solving PDEs with a large number of degrees of freedom (DOFs) can become a significant obstacle, even with high-performance computer hardware and computer-aided engineering (CAE) software. Although constructing a computational mesh in an adaptive manner can solve some of these problems, some applications require uniform high-fidelity meshes to solve physics problems, such as high-frequency wave propagation problems, fluid mechanics at high Reynolds numbers, and microscale (or multiscale) structural problems.

Driven by the desire to solve increasingly large and complex topology optimization problems without modifying the mesh, engineers have developed a variety of techniques

Responsible Editor: Xu Guo

✉ Gil Ho Yoon
ghy@hanyang.ac.kr

[1] Mechanical Engineering, Hanyang University, Seoul, Republic of Korea

Published online: 27 February 2024

(see Table 1). As the first approach to solve large-scale TO problems, mathematicians and engineers tried to replace the direct solvers, variants of the Gaussian factorization, with iterative solvers such as conjugate gradient (CG) [11 13], MINRES and GMRES (Amir and Sigmund 2011; Amir et al. 2010). In the parallel computing approach, the problem is divided into subdomains that are solved by iterative solver using different processors, whereas the interface coupling problem is solved using the local solutions at subdomain levels. The best known and perhaps the most promising parallel solvers belonging to the class of domain decomposition methods would be Schur complement (Noor et al. 1978), Gaussian elimination (Wilson 1974), and finite element tearing and interconnection solver (FETI) (Farhat and Roux 1991). Those methods are widely adopted by the scientific computing community and introduced to the topology optimization community (Evgrafov et al. 2008; Wadbro and Berggren 2009; Schmidt and Schulz 2011; Aage and Lazarov 2013; Aage et al. 2015, 2017). Since Evgrafov's the pioneering research on the advantages and difficulties of large-scale TO with a parallel solver, this parallel computing method has become a canonical approach in developing solutions for large-scale TO (Evgrafov et al. 2008; Aage et al. 2015, 2017).

Alternatively, one can opt for model reduction (MR) as an indirect approach for the computational efficiency of an analysis in the context of TO (Irons 1965; Yoon 2010; Ma et al. 1993; Jensen 2007; Cornwell et al. 1983; Liu et al. 2015; Zhao et al. 2018). MR methods have been utilized to solve dynamic problems that require iterative calculation of the system response at each time (or frequency) step. To the best of our knowledge, Ma was the first to introduce the mode superposition (MS) method, the oldest and most widely used MR technique, to a dynamic compliance minimization problem within the framework of the homogenization-based topology; they discussed the representation error of the original FRF using the MS method (Ma et al. 1993). After the first attempt, various MR methods, such as the modal displacement method, the modal acceleration method (Cornwell et al. 1983) are applied for efficient dynamic TO problems. Alternatively, a reanalysis-based approximation method is used which determines the structural response after any topological change using the initial (or previous) response of the structure. The reduction basis in reanalysis-based approximation is obtained within the Krylov subspace spanned by initial response using iterative solvers. There are several ways based on Krylov subspace methods such as the Ritz vector, hybrid Proper Orthogonal Decomposition and so on (Yoon 2010; Carlberg et al. 2016; Amir 2015; Choi et al. 2019).

Even with the above direct and indirect approaches, dynamic TO for extremely large-scale structures remains challenging. Based on our observations, certain iterative solvers tend to become ill-conditioned in both the context of a large-scale mesh and during the late stages of the optimization process. This tendency can occasionally impede the straightforward applicability of iterative solvers to problems involving large-scale optimization. In the case of the dynamic TO in the frequency domain, not only ill-conditioned system matrices resulting from Solid Isotropic Material with Penalization (SIMP) and stiff/void materials but also dynamic system matrices around resonance frequency deteriorate the numerical scalability, and thus completely different preconditioning strategies are required to keep CG solvers numerically scalable in the frequency response solver and the optimization iteration. Also, it's worth considering that certain modal-based reduction methods might face limitations when applied to the context of large-scale

Table 1 Representative studies and their system size of topology optimization problems solved in recent years

Year	References	Max #DOFs	System
2001	Sigmund (2001)	2.40 E+03	2D static compliance
2004	Kim et al. (2004)	4.07 E+06	3D static compliance
2005	Vemaganti and Lawrence (2005)	1.15 E+05	3D static compliance
2006	Mahdavi et al. (2006)	2.56 E+04	2D static compliance
2007	Wang et al. (2007)	1.01 E+06	3D static compliance
2008	Evgrafov et al. (2008)	1.54 E+06	2D and 3D static compliance
2009	Wadbro and Berggren (2009)	4.41 E+06	2D static (thermal) compliance
2011	Schmidt and Schulz (2011)	1.07 E+07	3D static compliance
2013	Aage and Lazarov (2013)	1.47 E+07	3D static compliance
2015	Alexandersen et al. (2016)	3.30 E+08	3D static (thermal) compliance
2017	Aage et al. (2017)	4.30 E+08	3D static compliance
2020	Kang et al. (2020)	2.45 E+06	3D eigenfrequency
2021	Träff et al. (2021)	6.98 E+07	3D static compliance
2021	Li et al. (2021)	2.93 E+05	2D and 3D dynamic compliance
2022	Kristiansen and Aage (2022)	8.1 E+06	3D dynamic compliance

topology optimization. This stems from the inherent challenge of conducting modal analyses within systems of significant scale. For this reason, TO methods for large-scale dynamic systems have rarely been studied compared to static systems (see Table 1).

Meanwhile, the *partial* design problem in this paper refers to a design case in which the design domain is only a part (or parts) of the whole analysis domain, as is common in many engineering design disciplines, i.e., a case in which the global (analysis) domain is composed of multiple design and non-design domains. The partial design problem can be easily found in various engineering problems because most engineering designers would want to have more control over the substructures so that they can select the proper design domain based on their realistic requirements, constraints, and further reflect their valuable intuition and experience into the optimization design process. One obstacle in the partial design problem is that the state (e.g., displacement, pressure, temperature etc.) and the design variables in the non-design domain as well as the design domain should be obtained for the optimization. Static condensation, which is the *physical coordinate*-based reduction scheme, is a common approach to eliminate those variables in non-design domain (Botkin and Yang 1991). However, even if the inaccuracy problem in the dynamic analysis is excluded, the static condensation method has the same limitation as general model reduction approaches because a reduction basis of static condensation is derived from the inverse of the stiffness matrix in the non-design domain.

To overcome these difficulties, we first introduce a concept of dynamic substructuring (or simply substructuring) with a repetitive geometry into the SIMP and density-based TO. The substructuring approach which was derived from both the idea of the *domain decomposition* and the *model reduction* is a way to obtain the approximated substructural dynamic behavior of large and/or complex structures by dividing them into several smaller and/or simpler interconnected substructures of which the dynamic behavior is much easier to obtain. The dynamic behavior of the entire structure is then obtained by assembling these dynamic behaviors of substructures. The schematic diagram of TO using the substructuring approach is shown in Fig. 1. After the first substructuring ideas were developed by the paper of Hurty in 1960 (Hurty Walter 1960), various attempts had followed resulting in the milestone methods by (Craig and Bampton 1968), (Rubin 1975) and (MacNeal 1971) in the 1960s and 1970s.

The paper also introduces the idea of repetitive geometry, which has been widely utilized for the homogenization of multi-scale problem or the periodically multi-partitioned problem (Zhang and Sun 2006; Wu et al. 2019), to create, memorize, and reduce the large-scale subsystem in the non-design domain. The FE models in the non-design domain are split and omitted by the idea of repetitive geometry, while the FE models in the design domain remain intact. This efficiently reduces the size of large scaled system in non-design domain and eliminates the need to obtain a response of the whole system for partial TO. Although the substructuring approach had been reported in a previous study by Kikuchi and Ma. (Ma et al. 2005), the detail process of methodology to introduce substructuring technique into the framework of topology optimization had not been clearly demonstrated, and following studies, especially on the large-scale TO for dynamic problems are lacking. This paper provides a detailed methodology to introduce the substructuring technique into the framework of topology optimization, specifically for dynamic problems. Additionally, the paper provides an example of the substructuring approach for partial topology optimization of a stiff structure in the frequency domain.

Thus, we first review the general framework of the TO, MR, and substructuring, then establish the framework of partial TO with the substructuring approach, and finally present a new method using the idea of repetitive geometry for large-scale TO problems. In Sect. 2, the basic concepts of the TO, the model reduction and the domain decomposition techniques are reviewed. In Sect. 3, we present a new TO procedure utilizing the concept of substructuring. Section 4 is dedicated to solving large-scale TO problems to illustrate the performance and capabilities of the present method, comparing with other conventional TO framework with MR

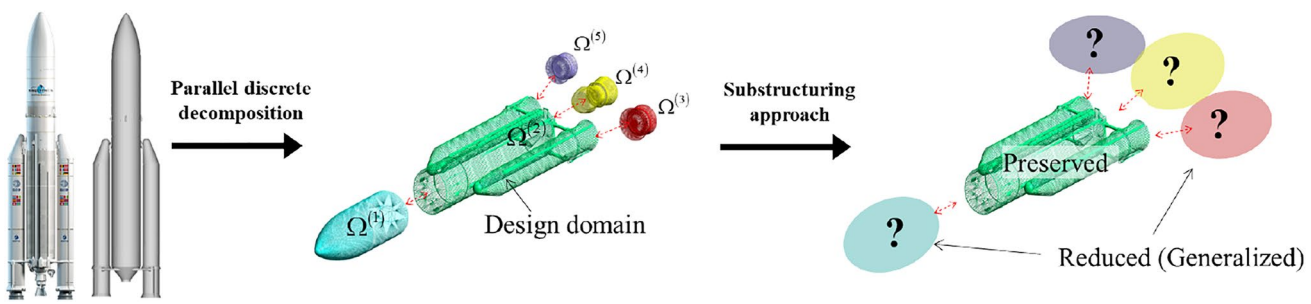

Fig. 1 Schematic diagram of substructuring approach for topology optimization of Arian V (https://www.arianespace.com/vehicle/ariane-5/)

scheme. The concluding section summarizes the findings and future research topics.

2 Overview of topology optimization using model reduction approach

This section briefly reviews the finite elements of formulation of the linear dynamic problem in frequency domain and the basic concept of the model reduction approach.

2.1 Equilibrium equations of a dynamic system

Newton's second equation is solved for the time-varying response of a linear solid structure with a time-varying force $\mathbf{f}(t)$, such that:

$$\mathbf{M}\ddot{\mathbf{u}}(t) + \mathbf{C}\dot{\mathbf{u}}(t) + \mathbf{K}\mathbf{u}(t) = \mathbf{f}(t) \tag{1}$$

where $\mathbf{M}$, $\mathbf{C}$, and $\mathbf{K}$ are the assembled mass, damping, and stiffness matrices with appropriate boundary conditions(Bathe 2006), respectively. The time-varying displacement, velocity, and acceleration vectors are represented by $\mathbf{u}(t)$, $\dot{\mathbf{u}}(t)$, and $\ddot{\mathbf{u}}(t)$, respectively. In this paper the viscous damping matrix $\mathbf{C}$ can be written as the case of proportional damping $\mathbf{C} = \alpha\mathbf{M} + \beta\mathbf{K}$ where α and β is damping coefficient. Assuming the harmonic response and excitation $\mathbf{u}(t) = \mathbf{u}e^{i\omega t}$, $\mathbf{f}(t) = \mathbf{f}e^{i\omega t}$, the following dynamic stiffness matrix $\mathbf{S}$ can be defined for the solution in the frequency space.

$$\mathbf{S}(\omega) = \mathbf{K} + i\omega\mathbf{C} - \omega^2\mathbf{M} \text{ and } \mathbf{u} = \mathbf{S}(\omega)^{-1}\mathbf{f} \tag{2}$$

2.2 General framework of the topology optimization

For the TO-based on the Solid Isotropic Material with Penalization (SIMP) approach a variable $\gamma \in L^{\infty}(\Omega)$ in design domain $\Omega \in \mathbb{R}^d$ plays a role of the design being optimized. Generally, the design variable $\gamma \in [0,\ 1]$,which called structural density, is introduced to control the material distribution in Ω through the interpolation function:

$$E(\gamma) = E_{\min} + \gamma^{p_k}\left(E_0 - E_{\min}\right),\ \rho(\gamma) = \rho_0\gamma^{p_m} \tag{3}$$

The nominal Young's modulus and the structural density are E_0 and ρ_0, respectively and the stiffness and mass penalty number are denoted by p_k and p_m. Also $E_{\min} \approx 10^{-9} \times E_0$ represents a lower bound of Young's modulus for void element. The linear dynamic Eq. (1), boundary conditions and material interpolation function (3) are all discretized into *NE* finite elements:

$$\mathbf{K} = \sum_{e=1}^{NE} \mathbf{k}_e \cdot E(\gamma_e), \mathbf{M} = \sum_{e=1}^{NE} \mathbf{m}_e \cdot \gamma_e^{p_m} \tag{4}$$

$$\begin{aligned} &\mathbf{k}_e = \int_{\Omega_e} \mathbf{B}^{\mathrm{T}}\mathbf{D}\mathbf{B}d\Omega\,,\ \mathbf{m}_e = \int_{\Omega_e} \rho_0\mathbf{H}^{\mathrm{T}}\mathbf{H}d\Omega, \\ &\mathbf{D} = \frac{E_0}{1-\nu^2}\begin{bmatrix} 1 & \nu & 0 \\ \nu & 1 & 0 \\ 0 & 0 & (1-\nu)/2 \end{bmatrix} \end{aligned} \tag{5}$$

where the stiffness and mass matrices of e-th element in the domain Ω_e are $\mathbf{k}_e$ and $\mathbf{m}_e$, respectively. The shape function, strain–displacement matrix, and constitutive matrix with a Poisson's ratio ν are denoted by $\mathbf{H}$, $\mathbf{B}$, and $\mathbf{D}$.

In many practical applications (linearized elastic, liner wave propagation, heat transfer, and stokes flow), a topology optimization problem can be formulated as:

$$\begin{aligned} \underset{\boldsymbol{\gamma}}{\text{Minimize}} \quad & f(\boldsymbol{\gamma}, \mathbf{u}) \\ \text{Subject to} \quad & \text{(state equations)} \\ & g(\boldsymbol{\gamma}, \mathbf{u}) \le 0 \\ & 0 \le \gamma_e \le 1\ \forall e \in \{1, 2, ..., NE\} \end{aligned} \tag{6}$$

where $f = f(\boldsymbol{\gamma}, \mathbf{u})$ denotes the objective function satisfying the state equation for the problem, which can be the static (and dynamic) compilation(Bendsøe and Kikuchi 1988; Ma et al. 1993, 1995) in this study, the mean eigenvalue(Ma et al. 1994; Pedersen 2000), deformation(compliant mechanism)(Kikuchi et al. 1998; Nishiwaki et al. 1998), stress value(Le et al. 2010; Yang and Chen 1996; Yoon 2014) or any others; $g = g(\boldsymbol{\gamma}, \mathbf{u})$ denotes the constraint function; $\boldsymbol{\gamma} = \left\{\gamma_1, \gamma_2, ..., \gamma_{NE}\right\}^{\mathrm{T}}$ denotes the vector of the design variables;.

2.3 Method of the domain decomposition

An idea of domain decomposition, the foundation of modern parallel computing and substructuring, has been the root of various methods for solving ever larger and more complex problems. To explain the principles of the domain decomposition scheme, we consider a finite element model defined on a global domain Ω, which is divided into N_s, each spanning a subdomain $\Omega^{(s)}$ and interface boundary Γ. For simplicity, the undamped equations of motion in subdomain $\Omega^{(s)}$ can be written as:

$$\mathbf{M}^{(s)}\ddot{\mathbf{u}}^{(s)} + \mathbf{K}^{(s)}\mathbf{u}^{(s)} = \mathbf{f}^{(s)} + \mathbf{g}^{(s)} \tag{7}$$

where the superscript $^{(s)}$ denotes the substructure s, and $\mathbf{g}^{(s)}$ is the vector of connecting (or interactional) force and/or moment with the neighboring substructures.

After generating the FE matrices in substructural level, each substructure was assembled under the following two conditions:

(1) Compatibility: the displacements of the substructures at the interface boundary DOFs must be identical
(2) Equilibrium: the sum of the interactional forces between neighboring substructures must be equal to zero

Now the s-th subdomain vectors and matrices are partitioned distinguishing the boundary and interior DOFs:

$$\mathbf{M}^{(s)} = \begin{bmatrix} \mathbf{M}_{ii} & \mathbf{M}_{ib} \\ \mathbf{M}_{bi} & \mathbf{M}_{bb} \end{bmatrix}^{(s)} \mathbf{K}^{(s)} = \begin{bmatrix} \mathbf{K}_{ii} & \mathbf{K}_{ib} \\ \mathbf{K}_{bi} & \mathbf{K}_{bb} \end{bmatrix}^{(s)}$$
$$\mathbf{u}^{(s)} = \begin{bmatrix} \mathbf{u}_i \\ \mathbf{u}_b \end{bmatrix}^{(s)} \mathbf{f}^{(s)} = \begin{bmatrix} \mathbf{f}_i \\ \mathbf{f}_b \end{bmatrix}^{(s)} \mathbf{g}^{(s)} = \begin{bmatrix} \mathbf{0} \\ \mathbf{g}_b \end{bmatrix}^{(s)} \tag{8}$$

where the subscript i and b denote the internal DOFs and the boundary DOFs, respectively. Following the equations of motion at the substructure level, the global equations of motion that have not yet been assembled can be expressed in the form of a block-diagonal matrix denoted by upper bar ($\bar{}$):

$$\overline{\mathbf{M}}\ddot{\overline{\mathbf{u}}} + \overline{\mathbf{K}}\overline{\mathbf{u}} = \overline{\mathbf{f}} + \overline{\mathbf{g}} \tag{9}$$

where,

$$\overline{\mathbf{M}} = \mathrm{diag}\left(\mathbf{M}^{(1)}, ..., \mathbf{M}^{(N_s)}\right) = \begin{bmatrix} \mathbf{M}^{(1)} & \cdots & \mathbf{0} \\ \vdots & \ddots & \vdots \\ \mathbf{0} & \cdots & \mathbf{M}^{(N_s)} \end{bmatrix},$$
$$\overline{\mathbf{K}} = \mathrm{diag}\left(\mathbf{K}^{(1)}, ..., \mathbf{K}^{(N_s)}\right), \tag{10}$$
$$\overline{\mathbf{u}} = \begin{bmatrix} \mathbf{u}^{(1)} \\ \vdots \\ \mathbf{u}^{(N_s)} \end{bmatrix}, \overline{\mathbf{f}} = \begin{bmatrix} \mathbf{f}^{(1)} \\ \vdots \\ \mathbf{f}^{(N_s)} \end{bmatrix}, \overline{\mathbf{g}} = \begin{bmatrix} \mathbf{g}^{(1)} \\ \vdots \\ \mathbf{g}^{(N_s)} \end{bmatrix}.$$

Note that by definition of Eq. (9,10), the FE matrices have duplicate interface DOFs. Next, the compatibility condition can be written in matrix form as:

$$\mathbf{B}\overline{\mathbf{u}} = \mathbf{0} \text{ or } \begin{bmatrix} \mathbf{0} & \mathbf{B}_b \end{bmatrix} \begin{bmatrix} \overline{\mathbf{u}}_i \\ \overline{\mathbf{u}}_b \end{bmatrix} = \mathbf{0} \tag{11}$$

where $\mathbf{B}$ is a signed Boolean matrix (if the interface DOFs match with each other) operating on the interface DOFs of the substructures. The rows of $\mathbf{B}$ state that any pair of matching interface DOFs $u_b^{(k)}$ and $u_b^{(l)}$ must have the same displacement, that is, $u_b^{(k)} - u_b^{(l)} = 0$.

Similar to the compatibility condition, the equilibrium condition can be written as:

$$\mathbf{L}^{\mathrm{T}}\overline{\mathbf{g}} = \mathbf{0} \text{ or } \begin{bmatrix} \mathbf{0} & \mathbf{L}_b^{\mathrm{T}} \end{bmatrix} \begin{bmatrix} \mathbf{0} \\ \overline{\mathbf{g}}_b \end{bmatrix} = \mathbf{0} \tag{12}$$

where $\mathbf{L}$ is a Boolean matrix localizing the interface DOF of the substructures in the dual set of DOFs. The columns of $\mathbf{L}$ state that the sum of any pair of interface connecting forces $g_b^{(k)}$ and $g_b^{(l)}$ is equal to zero, that is, $g_b^{(k)} + g_b^{(l)} = 0$.

Now, the total system can be described by above Eqs. (9–12):

$$\begin{cases} \overline{\mathbf{M}}\ddot{\overline{\mathbf{u}}} + \overline{\mathbf{K}}\overline{\mathbf{u}} = \overline{\mathbf{f}} + \overline{\mathbf{g}} \\ \mathbf{B}\overline{\mathbf{u}} = \mathbf{0} \\ \mathbf{L}^{\mathrm{T}}\overline{\mathbf{g}} = \mathbf{0} \end{cases} \tag{13}$$

Mathematically, an assembled FE model is obtained by following statements:

$$\overline{\mathbf{u}} = \mathbf{L}\mathbf{u} \tag{14}$$

$$\overline{\mathbf{g}} = -\mathbf{B}^{\mathrm{T}}\boldsymbol{\lambda} \tag{5}$$

where $\mathbf{u}$ represents the unique set of interface DOFs for the assembled system and $\boldsymbol{\lambda}$ are the Lagrange multipliers of d'Alembert's principle of virtual work, corresponding physically to the connecting (constraining) force intensity (see Lagrange multiplier field in Fig. 2). Using this statement in Eq. (14), the compatibility condition of Eq. (11) is satisfied for any set of $\mathbf{u}$ (i.e.,$\mathbf{BLu} = \mathbf{0}\,\forall\mathbf{u}$). Hence, the two Boolean matrices represent each other's null space, namely, $\mathbf{L} = \mathrm{null}(\mathbf{B})$, $\mathbf{B}^{\mathrm{T}} = \mathrm{null}\left(\mathbf{L}^{\mathrm{T}}\right)\mathbf{B}^{\mathrm{T}} = \mathrm{null}\left(\mathbf{L}^{\mathrm{T}}\right)$. Consequently, the global system in Eq. (7) can be described as "*dual form*":

$$\begin{cases} \overline{\mathbf{M}}\ddot{\overline{\mathbf{u}}} + \overline{\mathbf{K}}\overline{\mathbf{u}} = \overline{\mathbf{f}} - \mathbf{B}^{\mathrm{T}}\boldsymbol{\lambda}, \\ \mathbf{B}\overline{\mathbf{u}} = \mathbf{0} \end{cases}$$
$$\text{or } \begin{bmatrix} \overline{\mathbf{M}} & \mathbf{0} \\ \mathbf{0} & \mathbf{0} \end{bmatrix} \begin{bmatrix} \ddot{\overline{\mathbf{u}}} \\ \boldsymbol{\lambda} \end{bmatrix} + \begin{bmatrix} \overline{\mathbf{K}} & \mathbf{B} \\ \mathbf{B}^{\mathrm{T}} & \mathbf{0} \end{bmatrix} \begin{bmatrix} \overline{\mathbf{u}} \\ \boldsymbol{\lambda} \end{bmatrix} = \begin{bmatrix} \overline{\mathbf{f}} \\ \mathbf{0} \end{bmatrix}. \tag{16}$$

Now one can solve the subdomain problems in parallel by knowing $\overline{\mathbf{u}}_b$ and $\boldsymbol{\lambda}$, which can be obtained by solving coarse boundary problem, $\overline{\mathbf{K}}_{bb} = \mathbf{B}_b^{\mathrm{T}}\boldsymbol{\lambda} - \overline{\mathbf{f}}_b$. This *dual* approach led to the parallel solvers for FEM known as dual Schur complement methods of FETI (finite elements tearing and interconnecting) (Noor et al. 1978). Meanwhile a "*primal form*" can be written by the choice of DOFs in the unique set $\mathbf{u}$:

$$\mathbf{M}\ddot{\mathbf{u}} + \mathbf{K}\mathbf{u} = \mathbf{f} \tag{17}$$

where,

$$\mathbf{M} = \mathbf{L}^{\mathrm{T}}\overline{\mathbf{M}}\mathbf{L},\ \mathbf{K} = \mathbf{L}^{\mathrm{T}}\overline{\mathbf{K}}\mathbf{L},\ \mathbf{f} = \mathbf{L}^{\mathrm{T}}\overline{\mathbf{f}} \tag{18}$$

A *primal* or *dual*-assembled system is obtained depending on whether a compatibility or equilibrium condition is

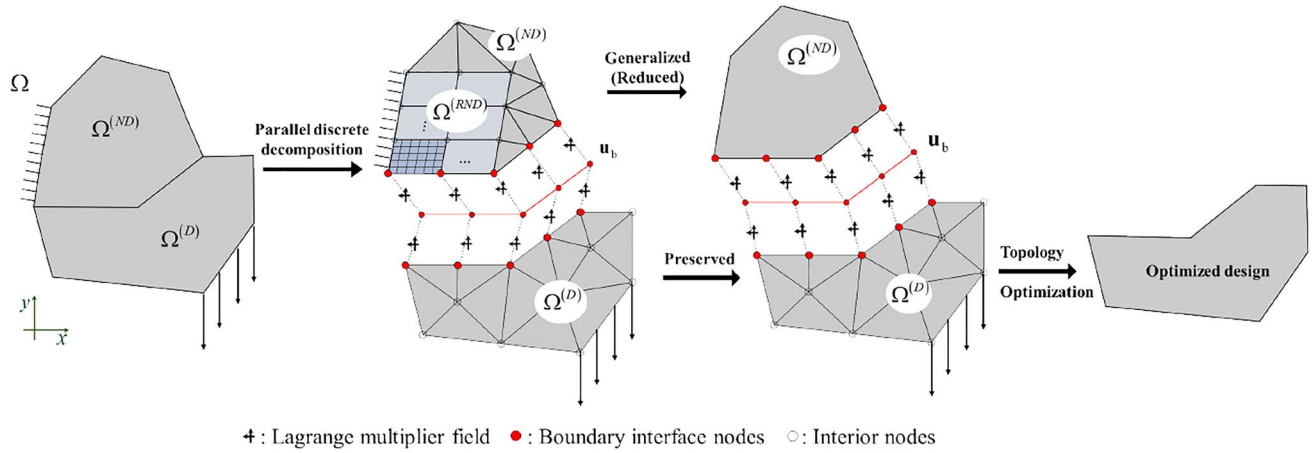

Fig. 2 Schematic diagram of partial topology optimization applying substructuring

satisfied a priori. More details of the general framework of substructure assembly are comprehensively documented in the work of Kleck and Rixen(Klerk et al. 2008).

2.4 General framework of the model reduction scheme for optimization problem

The computing power has significantly increased since the emergence of TO. But even by the most advanced and state-of-the-art computational systems, it is still a challenging to obtain TO solution within moderate computation cost and time because one should iteratively calculate the response of the large-scale system during optimization process. These difficulties could be simply overcome by constructing coarser mesh, but more precise and sophisticated optimization design is required with the development of manufacturing technology. Therefore, a method that reduces the dynamic problem without modifying the mesh is necessary. Such methods are called model order reduction, in which the full set of DOFs (physical space) is approximated by a set of possible displacement shapes and corresponding amplitudes called the generalized DOFs (generalized space). Using a proper transformation matrix $\mathbf{R}$, also called a *reduction basis*, the approximated displacement vector $\tilde{\mathbf{u}}$ of the original displacement vector $\mathbf{u}$ and its generalized coordinate $\mathbf{q}$ can be defined as:

$$\mathbf{u} \approx \tilde{\mathbf{u}} = \mathbf{R}\mathbf{q} \tag{19}$$

For a system with N degrees of freedom, $\mathbf{R} \in \mathbb{R}^{N \times M} (N > M)$ where m is dimension of approximated model. All kinds of structural modes (i.e., eigenmodes, static modes, interface modes, approximated modes, etc.) can be used to generate the reduction basis $\mathbf{R}$. For example, if a reduction basis is created by the eigenmodes, the method is called the mode superposition (MS) method. The equations of motion in Eq. (1), except for damping, can be written as:

$$\mathbf{M}\mathbf{R}\ddot{\mathbf{q}} + \mathbf{K}\mathbf{R}\mathbf{q} = \mathbf{f} + \mathbf{r} \tag{20}$$

where $\mathbf{r}$ is the error or residual load because the generalized DOFs do not span the entire solution space; it represents the approximation error in Eq. (19). The inner product of $\mathbf{r}$ with any subspace spanned by the reduction basis $\mathbf{R}$ is zero because the error represents the part of the equation that lies outside the subspace of the reduction basis (i.e., $\mathbf{R}^{\mathrm{T}}\mathbf{r} = \mathbf{0}$). Using this property, the reduced equations of motion denoted by tilde (˜) can be expressed as follows:

$$\tilde{\mathbf{M}}\ddot{\mathbf{q}} + \tilde{\mathbf{K}}\mathbf{q} = \tilde{\mathbf{f}} \tag{21}$$

where,

$$\begin{cases} \tilde{\mathbf{M}} = \mathbf{R}^{\mathrm{T}}\mathbf{M}\mathbf{R} \\ \tilde{\mathbf{K}} = \mathbf{R}^{\mathrm{T}}\mathbf{K}\mathbf{R} \\ \tilde{\mathbf{f}} = \mathbf{R}^{\mathrm{T}}\mathbf{f} \\ \tilde{\mathbf{g}} = \mathbf{R}^{\mathrm{T}}\mathbf{g} \end{cases} \tag{22}$$

Now the system size reduced from $N \times N$ to $M \times M$. After solving the above reduced system for the generalized coordinate $\mathbf{q}$, the approximated solution $\tilde{\mathbf{u}}$ can be obtained using Eq. (19), which is generally referred to as the recovery process in MR approach. The optimization formulations (6) are approximated by replacing the exact solution $\mathbf{u}$ with approximated solution $\tilde{\mathbf{u}}$ and the computational cost can be reduced by obtaining the responses of the reduced order system instead of full order system. Note that the model reduction approach does not always guarantee lower computational costs because the reduction basis must be iteratively updated as the topological shape changes during the optimization process.

3 Solutions in the framework of substructuring for partial topology optimization of large FE model

3.1 Framework of partial topology optimization in frequency domain

The *partial* design problem refers to cases where the design domain and the analysis domain do not match, which can be easily found in various engineering problems. In contrast to conventional single domain TO, in which a given amount of the material is assigned to the entire analysis domain, partial TO allows the designer to assign different amounts of the material, or even different materials, to the various subdomains of the structure while keeping the non-design domain intact. For example, Fig. 2 depicts the 'structure fixture simultaneous design' where a global domain that is divided into two subdomains, where the model in non-design domain is not changed during optimization process. In general, a partial TO problem is defined as a TO problem that has multiple subdomains and only some of the subdomains are design domains. The objective function of the partial TO problem can be related to the performance/functionality of the entire analysis domain or to that of a single domain or of multiple domains considered in the design problem. Now the partial TO problem of a random stiff structure in frequency domain can be formulated by following statements:

$$\begin{aligned} \underset{\boldsymbol{\gamma}}{\text{Minimize}} \quad & f = \sum_{s=1}^{N_s} w^{(s)} \cdot f^{(s)}(\boldsymbol{\gamma}, \mathbf{u}) \\ \text{Subject to} \quad & \mathbf{S}\mathbf{u} = \mathbf{f} \\ & g^{(s)}(\boldsymbol{\gamma}, \mathbf{u}) \leq 0 \; \forall s \in \left\{1, 2, ..., N_s\right\} \\ & 0 \leq \gamma(\mathbf{r}) \leq 1 \; \forall \mathbf{r} \in \Omega^{(D)} \end{aligned} \tag{23}$$

where $f^{(s)}$,$w^{(s)}$ and $g^{(s)}$ denotes the s-th objective, weight and constraint function for the s-th substructure in the s-th subdomain out of a total of N_s subdomains in the design domain $\Omega^{(D)} \subseteq \Omega$, respectively; $\boldsymbol{\gamma} = \left\{\gamma_1, \gamma_2, ..., \gamma_{NE}\right\}^{\mathrm{T}}$ denotes the vector of the design variables.

3.2 Introduction of new topology optimization frameworks using substructuring approach

The TO framework using MR approach, described in the previous Sect. 2.4, still has some limitations for partial design problems of large-scale models: (1) The process of finding a basis, such as eigen-analysis or Krylov expansion, generally requires more computational power than the process of obtaining a static solution. In scenarios where the problem size expands to an extent where the attainment of a static solution becomes elusive, the quest for a suitable reduction basis could potentially face challenges. This prompts a consideration of the adaptability of the MR approach within the domain of static optimization problems; (2) The reduction basis should be recalculated with each iteration as the topological shape changes during the optimization process. Even in the dynamic problem, the MR approach is not suitable because this kind of overhead could outweigh the benefits of order reduction; (3) Even if the responses of the reduced system can be obtained using MR schemes, the responses should be recovered to the original large system to obtain objective and sensitivity values for the TO.

A substructuring approach, which is a method of partitioning, reducing, and assembling models, could be much more effective than conventional MR schemes for partial optimization problems. The substructuring approach can be broadly divided into a top-down style and a bottom-up style. The former, such as FETI mentioned in Sect. 2.3, directly generates a global system (or global model, global FE matrix) and splits the global system into subdomain (or substructural) systems, while the latter generates the subdomain systems respectively and assembles those systems into the global level after reduction. In this study, the bottom-up approach is used for partial topology optimization to avoid handling the full order global matrix.

To explain the concept of the TO using a substructuring scheme, let us consider the equations of motion in Eq. (7) again. Using the generalized set of DOFs in Eq. (19), the system in Eq. (7) can be reduced:

$$\tilde{\mathbf{M}}^{(s)}\ddot{\tilde{\mathbf{q}}}^{(s)} + \tilde{\mathbf{K}}^{(s)}\mathbf{q}^{(s)} = \tilde{\mathbf{f}}^{(s)} + \tilde{\mathbf{g}}^{(s)} \tag{24}$$

where,

$$\begin{cases} \tilde{\mathbf{M}}^{(s)} = \mathbf{R}^{(s)\mathrm{T}}\mathbf{M}^{(s)}\mathbf{R}^{(s)} \\ \tilde{\mathbf{K}}^{(s)} = \mathbf{R}^{(s)\mathrm{T}}\mathbf{K}^{(s)}\mathbf{R}^{(s)} \\ \tilde{\mathbf{f}}^{(s)} = \mathbf{R}^{(s)\mathrm{T}}\mathbf{f}^{(s)} \\ \tilde{\mathbf{g}}^{(s)} = \mathbf{R}^{(s)\mathrm{T}}\mathbf{g}^{(s)} \end{cases} \tag{25}$$

For a common denominator for the coupling substructures, the DOFs on the boundaries of the substructures are preserved, and only the DOFs on the internal substructures $\mathbf{u}_i^{(s)}$ are reduced to a generalized coordinate $\mathbf{q}^{(s)}$. Therefore, the approximated equations of motion in Eq. (19) are:

$$\begin{bmatrix} \mathbf{u}_i \\ \mathbf{u}_b \end{bmatrix}^{(s)} \approx \begin{bmatrix} \mathbf{R}_i \\ \mathbf{R}_b \end{bmatrix}^{(s)} \mathbf{q}^{(s)} \text{ where } \mathbf{q}^{(s)} = \begin{bmatrix} \mathbf{q}_i \\ \mathbf{q}_b = \mathbf{u}_b \end{bmatrix}^{(s)} \tag{26}$$

It is to be noted that the superscript $^{(s)}$ is not explicitly shown for following equations to minimize notational clutter. To avoid confusion, it is explicitly mentioned when the global matrix is considered along with substructural matrix. In general, two types of component modes are considered for a reduction basis $\mathbf{R}$ for substructuring: dynamic and static mode. The former mode accounts for the dynamic behavior

of the substructure, whereas the latter mode accounts for the interaction between neighboring substructures, ensuring that compatibility conditions after assembly are satisfied:

$$\mathbf{u} = \mathbf{u}_{dyn} + \mathbf{u}_{stat} \tag{27}$$

Since the substructuring was introduced in the finite element method, tremendous number of methods have been developed to create a more accurate and robust reduction basis, in this study the earliest method introduced by Craig and Bampton is adopted because of its simplicity and reliability. The Craig-Bampton (CB) method utilizes *internal vibration mode* (eigenmode) and *constraint mode* as the dynamic and static mode, respectively in Eq. (27). The former is obtained by solving the eigenvalue problem of the substructure fixed on its interface boundary, while the latter is defined as a unit displacement on one boundary DOF keeping all others fixed. Both modes can be obtained based on the above statement in Eq. (8):

$$\left(\mathbf{K}_{ii} - \omega_{i,j}^2 \mathbf{M}_{ii}\right)\phi_{i,j} = \mathbf{0},\ \mathbf{\Phi}_i = \left[\phi_1, \phi_2, ...\right],\ \mathbf{\Phi} = \begin{bmatrix} \mathbf{\Phi}_i \\ \mathbf{0} \end{bmatrix} \tag{28}$$

$$\mathbf{\Psi} = \begin{bmatrix} \mathbf{\Psi}_i \\ \mathbf{\Psi}_b \end{bmatrix} = \begin{bmatrix} -\mathbf{K}_{ii}^{-1}\mathbf{K}_{ib} \\ \mathbf{I} \end{bmatrix} \tag{29}$$

Here $\omega_{i,j}$ and $\phi_{i,j}$ are the j^{th} eigenfrequency and associated eigenmode of the internal substructure, respectively, while a set of internal vibration modes and constraint modes are denoted by $\mathbf{\Phi}_i$ and $\mathbf{\Psi}_c$, respectively. Now, we can obtain the following approximate displacement:

$$\mathbf{u} = \mathbf{u}_{dyn} + \mathbf{u}_{stat} \simeq \mathbf{\Phi\eta} + \mathbf{\Psi u}_b \tag{30}$$

or

$$\mathbf{u} = \begin{bmatrix} \mathbf{u}_i \\ \mathbf{u}_b \end{bmatrix} \simeq \tilde{\mathbf{u}} = \begin{bmatrix} \mathbf{\Phi}_i & \mathbf{\Psi}_i \\ \mathbf{0} & \mathbf{I} \end{bmatrix} \begin{bmatrix} \mathbf{\eta}_i \\ \mathbf{u}_b \end{bmatrix} = \mathbf{Rq} \tag{31}$$

Here a problem is the system on the interior DOFs is so large that one cannot conduct the process to obtain these modes. To solve this problem, an idea of repetitive partitioning is introduced. In our presented method the non-design domain is partitioned into the repetitive partitions of the same discretization and the rest of the partitions as show in Fig. 2. As a result, FE model in large-scale non-design is constructed only by a single repetitive FE substructure(partition) and the residual. Now the reduced subsystems in Eq. (24) are assembled as *primal* form by same procedure in Sect. 2.3. The reduced equations of motion that have not yet been assembled can be expressed in the form of a block-diagonal matrix:

$$\bar{\tilde{\mathbf{M}}}\ddot{\bar{\mathbf{q}}} + \bar{\tilde{\mathbf{K}}}\bar{\mathbf{q}} = \bar{\tilde{\mathbf{f}}} + \bar{\tilde{\mathbf{g}}} \tag{32}$$

where,

$$\begin{aligned} \bar{\tilde{\mathbf{M}}} &= diag\left(\tilde{\mathbf{M}}^{(1)}, ..., \tilde{\mathbf{M}}^{(N_s)}\right), \\ \bar{\tilde{\mathbf{K}}} &= diag\left(\tilde{\mathbf{K}}^{(1)}, ..., \tilde{\mathbf{K}}^{(N_s)}\right), \\ \bar{\mathbf{q}} &= \left[\mathbf{q}^{(1)T}, ..., \mathbf{q}^{(N_s)T}\right]^T, \\ \bar{\tilde{\mathbf{f}}} &= \left[\tilde{\mathbf{f}}^{(1)T}, ..., \tilde{\mathbf{f}}^{(N_s)T}\right]^T, \\ \bar{\tilde{\mathbf{g}}} &= \left[\tilde{\mathbf{g}}^{(1)T}, ..., \tilde{\mathbf{g}}^{(N_s)T}\right] \end{aligned} \tag{33}$$

Now, $M \times M$ assembled reduced system ($N > M$) can be obtained by the compatibility condition and compatibility condition without the need to directly calculate the huge original total system matrices:

$$\tilde{\mathbf{M}}\ddot{\mathbf{q}} + \tilde{\mathbf{K}}\mathbf{q} = \tilde{\mathbf{f}} \text{ or } \tilde{\mathbf{S}}\mathbf{q} - \tilde{\mathbf{f}} = \mathbf{0} \tag{34}$$

where,

$$\mathbf{q} = \mathbf{L}\bar{\mathbf{q}},\ \tilde{\mathbf{M}} = \mathbf{L}^{\mathrm{T}}\bar{\tilde{\mathbf{M}}}\mathbf{L},\ \tilde{\mathbf{K}} = \mathbf{L}^{\mathrm{T}}\bar{\tilde{\mathbf{K}}}\mathbf{L},\ \tilde{\mathbf{f}} = \mathbf{L}^{\mathrm{T}}\bar{\tilde{\mathbf{f}}},\ \tilde{\mathbf{S}} = \left(\tilde{\mathbf{K}} - \omega^2\tilde{\mathbf{M}}\right) \tag{35}$$

On the other hand, the FE model in the design domain remains intact to avoid the disadvantages of the MR approach in optimization framework (It is noteworthy that the substructural model in design domain could be reduced by condensation approach that maintains physical meaning even after reduction, but this case will not be dealt with in order to clarify our idea). Therefore, the generalized(reduced) response by substructuring in Eq. (32) can be rewritten as:

$$\bar{\mathbf{q}} = \left[\boldsymbol{u}^{(D)T}, \boldsymbol{q}^{(ND)T}\right] = \left[\left\{\boldsymbol{u}_i^T, \boldsymbol{u}_b^T\right\}^{(D)}, \left\{\boldsymbol{q}_i^T, \boldsymbol{q}_b^T\right\}^{(ND)}\right]^T \tag{36}$$

$$\boldsymbol{q} = \mathbf{L}\bar{\mathbf{q}} = \left[\boldsymbol{u}^{(D)T}, \boldsymbol{q}_i^{(ND)T}\right]^T,\ \boldsymbol{u}_b^{(D)} = q_b^{(ND)} \tag{37}$$

Now, let us consider the optimization problem (23). In this paper, we consider following two objective functions proposed in works of Jacob (Amir et al. 2010) and Ma et al. (Evgrafov et al. 2008):

$$f_1 = \left|\mathbf{f}(\omega)^{\mathrm{T}}\mathbf{u}(\omega)\right| \text{ (mean} - \text{compliance minimization)} \tag{38}$$

$$\begin{aligned} f_2 &= \int_{\omega_s}^{\omega_s} f_1(\omega)\,\mathrm{d}\omega \\ &= \sum_i w_i f_1\left(\omega_i\right) \text{ (Dynamic} - \text{compliance minimization)} \end{aligned} \tag{39}$$

Here, mean-compliance f_1 is a function of the exciting frequency ω and dynamic-compliance f_2 is the integration of the objective function above within a certain frequency(angular

velocity) range $[\omega_s,\omega_e]$ and w_i, ω_i is the set of quadrature weights and points. Now, the Eqs. (38,39) can be written based on the relation in Eqs. (19,22) as follows:

$$f_1 \simeq \left|\tilde{\mathbf{f}}(\omega)^{\mathrm{T}}\mathbf{q}(\omega)\right| \tag{40}$$

$$f_2 \simeq \int_{\omega_s}^{\omega_s} \left|\tilde{\mathbf{f}}(\omega)^{\mathrm{T}}\mathbf{q}(\omega)\right| d\omega \tag{41}$$

Meanwhile, for the sensitivity value for the objective function and the constraint with respect to design variable $\boldsymbol{\gamma}$, the adjoint variable method (AVM) and Lagrange multiplier method are adopted. The sensitivity value in the static system can be derived via the followings:

$$\mathcal{L} = \mathbf{f}^{\mathrm{T}}\mathbf{u} + \boldsymbol{\lambda}^{\mathrm{T}}(\mathbf{K}\mathbf{u} - \mathbf{f}) \text{ (Lagrange equation)} \tag{42}$$

where Lagrange multiplier $\boldsymbol{\lambda}$ is the vector of adjoint variables. By differentiating the Lagrange equation $\mathcal{L}$ with respect to the design variable $\boldsymbol{\gamma}^{(D)}$ in design domain, the sensitivity can be obtained:

$$\begin{aligned}\frac{\mathrm{d}\mathcal{L}}{\mathrm{d}\boldsymbol{\gamma}^{(D)}} &= \left(2\mathbf{u}^{\mathrm{T}}\mathbf{K} + \boldsymbol{\lambda}^{\mathrm{T}}\mathbf{K}\right)\frac{\partial \mathbf{u}}{\partial \boldsymbol{\gamma}^{(D)}} + \mathbf{u}^{\mathrm{T}}\frac{\partial \mathbf{K}}{\partial \boldsymbol{\gamma}^{(D)}}\mathbf{u} + \boldsymbol{\lambda}^{\mathrm{T}}\frac{\partial \mathbf{K}}{\partial \boldsymbol{\gamma}^{(D)}}\mathbf{u} \\ &= -\mathbf{u}^{\mathrm{T}}\frac{\partial \mathbf{K}}{\partial \boldsymbol{\gamma}^{(D)}}\mathbf{u}\end{aligned} \tag{43}$$

where, $\boldsymbol{\lambda}^{\mathrm{T}} = -2\mathbf{u}^{\mathrm{T}}$. Meanwhile, the stiffness matrix $\mathbf{K}$ in Eq. (4) can be written as:

$$\begin{aligned}\mathbf{K} &= \sum_{e=1}^{NE^{(D)}} \left(\gamma_e\right)^{p_k} \cdot \mathbf{k}_e + \sum_{e=1}^{NE^{(ND)}} \left(\gamma_e\right)^{p_k} \cdot \mathbf{k}_e \\ &= \mathbf{K}_g^{(D)} + \mathbf{K}_g^{(D)}\end{aligned} \tag{44}$$

where,

$$\mathbf{K}_g^{(D)} = \sum_{e=1}^{NE^{(D)}} \left(\gamma_e\right)^{p_k} \cdot \mathbf{k}_e = \begin{bmatrix} \mathbf{K}^{(D)} & \mathbf{0} \\ \mathbf{0} & \mathbf{0} \end{bmatrix} \tag{45}$$

$$\mathbf{K}_g^{(D)} = \mathbf{N}^{(D)\mathrm{T}}\mathbf{K}^{(D)}\mathbf{N}^{(D)}, \tag{46}$$

$$\mathbf{u}^{(D)} = \mathbf{N}^{(D)}\mathbf{u}. \tag{47}$$

Here, $\mathbf{N}^{(D)}$ is the Boolean matrix that operate on the DOF associated with the elements within the design. The size of $\mathbf{K}_g^{(D)}$ is $N \times N$, equal to the global assembled system matrix and the size of $\mathbf{K}^{(D)}$ is $N_d \times N_d$, equal to the local subsystem matrix in the design domain. Also note that the system in non-design domain can be reduced by substructuring approach. Recalling the state variables in partially reduced system in Eq. (37), Boolean matrix for reduced system can be written as:

$$\mathbf{u}^{(D)} = \tilde{\mathbf{N}}^{(D)}\mathbf{q} \tag{48}$$

where, $\boldsymbol{q} = \left[\boldsymbol{u}^{(D)T}, \boldsymbol{q}_i^{(ND)T}\right]^T$.

Now the sensitivity equation in Eq. (43) would write:

$$\begin{aligned}\frac{\mathrm{d}\mathcal{L}}{\mathrm{d}\boldsymbol{\gamma}^{(D)}} &= -\mathbf{u}^{\mathrm{T}}\frac{\partial \mathbf{K}_g^{(D)}}{\partial \boldsymbol{\gamma}^{(D)}}\mathbf{u} \\ &= -\mathbf{u}^{(D)\mathrm{T}}\frac{\partial \mathbf{K}^{(D)}}{\partial \boldsymbol{\gamma}^{(D)}}\mathbf{u}^{(D)}\end{aligned} \tag{49}$$

Because the design variable $\boldsymbol{\gamma}$ is only in the design domain which is not generalized i.e.,$\boldsymbol{\gamma} = \boldsymbol{\gamma}^{(D)}$, Eq. (43) can be rewritten as:

$$\frac{d\mathcal{L}}{d\gamma} = -u^{(D)T}\frac{\partial K^{(D)}}{\partial \gamma^{(D)}}u^{(D)} \tag{50}$$

Accordingly, state variables in the non-design domain $\mathbf{u}^{(ND)}$ or $\mathbf{q}^{(ND)}$ are no longer required for sensitivity values and there is no need to calculate the reduction basis for every TO iteration because the FE model in non-design domain is not change. The schematic diagram of proposed method and optimization process is illustrated in Fig. 2 and Fig. 3.

Similarly, the sensitivity values of dynamic compliance f_1 and f_2 can be obtained as follows.

$$\frac{\mathrm{d}f_1}{\mathrm{d}\boldsymbol{\gamma}} = 2\mathrm{Real}\left(\boldsymbol{\lambda}^{\mathrm{T}}\left(\frac{\partial \mathbf{S}^{(D)}}{\partial \boldsymbol{\gamma}^{(D)}}\mathbf{u}^{(D)}\right)\right) \tag{51}$$

$$\frac{\mathrm{d}f_2}{\mathrm{d}\boldsymbol{\gamma}} = 2\int_{\omega_s}^{\omega_e} \mathrm{Real}\left(\boldsymbol{\lambda}^{\mathrm{T}}\left(\frac{\partial \mathbf{S}^{(D)}}{\partial \boldsymbol{\gamma}^{(D)}}\mathbf{u}^{(D)}\right)\right)\mathrm{d}\omega \tag{52}$$

$$\lambda = -\frac{1}{2}\mathrm{conj}(\mathbf{u}^{(D)}) \tag{53}$$

Here $\mathrm{conj}(\mathbf{u}^{(D)})$ denotes the complex conjugate of the state variables in the design domain.

4 Numerical examples

To illustrate the performance of substructuring approach for partial topology optimization applications, this section presents several numerical problems. All the optimization procedures are implemented in the framework of MATLAB (MATLAB 2022b, 64bit, Gold 6342 24 cores, 512 GB) and the design domains and material properties are arbitrary chosen without loss of generality. To solve the optimization problem, a mathematical optimization algorithm (method of moving asymptotes (MMA)) is employed here. For the convergence criteria of the large-scale optimization process, a small value of absolute

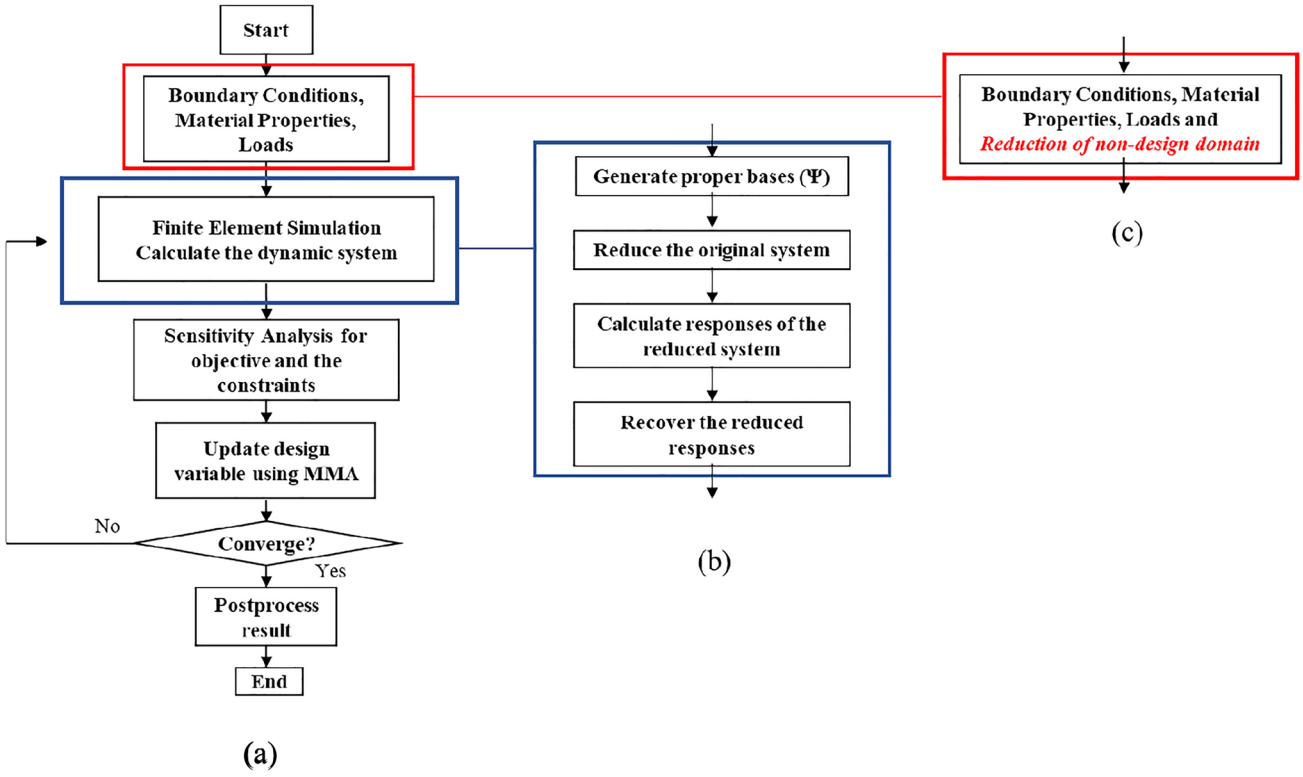

Fig. 3 Optimization processes **a** without MR schemes, **b** with conventional MR schemes and **c** with substructuring. Note that all processes associated with the model reduction are now conducted prior to the optimization iteration, which reduces the significant number of design variables. As a result, additional benefit can be expected; generally, when the eigenmode-based MR scheme is used for dynamic TO, mode switching phenomena among eigenfrequencies (Koh et al. 2020) or the localized eigenmodes occur during an optimization process (Yoon 2010; Pedersen 2000), which deteriorates the approximation accuracy of the FRFs and generates gray elements in optimized results. But the proposed approach, in which the model in design domain does not utilize eigenmodes, is no longer affected by these side effects

change of design variables and a large value of the maximum iteration are set compared to general optimization problems.

$$\max\left(\left|\boldsymbol{\gamma}_{\text{iter.}}-\boldsymbol{\gamma}_{\text{iter.}-1}\right|/\left|\boldsymbol{\gamma}_{\text{iter.}-1}\right|\right) < 10^{-3} \text{ and Maximum iteration } = 500 \tag{54}$$

where the iteration number is denoted by iter. Also we note that the eigenvalue problems for the presented examples are only partially solved by the Krylov–Schur algorithm (Stewart 2002) and thus, eigenmode selection methods, such as the frequency cutoff method, are substituted by the frequency response function(FRF) analysis.

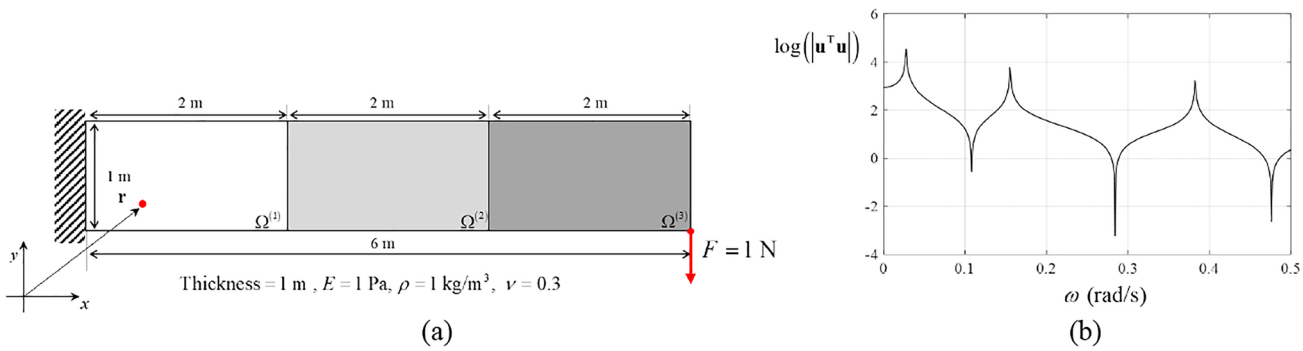

Fig. 4 Cantilever benchmark design problem. **a** Problem definition (Elastic modulus (E) = 1 Pa, density (ρ) = 1 kg/m^3, Poisson ratio (ν) = 0.3) and **b** Resulting frequency responses

In order to ensure existence of optimal design to the dynamic TO problem and prevent checkerboard patterns in the design, filtering method is used on the sensitivities of the objective function. It must be emphasized that the filter is essential to reduce the gray elements especially in the dynamic TO problems in practice. For TO problems having the multiple design domains, the filter can be given as:

$$\frac{\mathrm{d}\widehat{f}}{\mathrm{d}\gamma_k} = \frac{1}{\gamma_k \sum_{i=1}^{NE^{(D)}} H_i} \sum_{i=1}^{NE^{(D)}} H_i \gamma_k \frac{\mathrm{d}f}{\mathrm{d}\gamma_k},$$
$$H_i = \begin{cases} r_{\min} - \mathrm{dist}(k,i), \ \left\{ i \in NE^{(D)} \middle| \mathrm{dist}(k,i) \le r_{\min} \right\} \\ 0, \left\{ i \in NE^{(D)} \middle| \mathrm{dist}(k,i) > r_{\min} \right\} \end{cases} \text{(filtering within whole design domain} \tag{55}$$

where the operator dist(k,i) is defined as the distance between center of k-th element and i-th element and $r_{\min}$ is the radius of the circle that controls which sensitivities contribute to the filtering of the sensitivity with respect to the k-th design variable. Also,$NE^{(D)}$ is number of elements in the whole design domain.

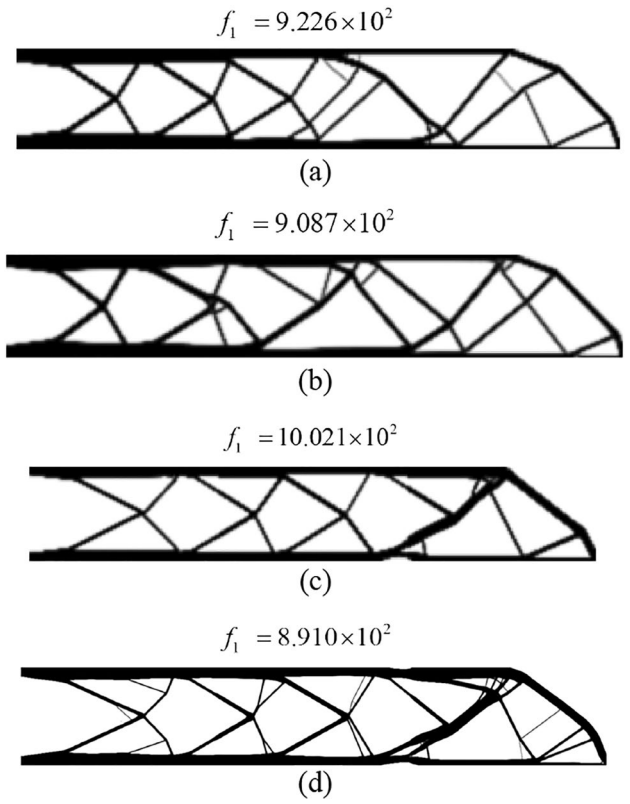

Fig. 5 Results of static compliance problem. Optimization layout of **a** conventional approach with single volume constraint ($V/V_0 < 0.3$, V_0 is initial volume), **b** substructuring approach with single volume constraint, **c** substructuring approach with multiple volume constraints ($V^{(k)}/V_0^{(k)} < 0.3$, $k=1,2,3$), and **d** substructuring approach with multiple volume constraints and refined mesh (element size = 0.005)

4.1 Cantilever beam problem

For the first example a cantilever beam with three subdomains ($\Omega^{(1)}$,$\Omega^{(2)}$,$\Omega^{(3)}$) in Fig. 4 is proposed to solve the structure-fixture simultaneous design considering dynamic compliance. The size of the beam is 6 m × 3 m having random material properties (Elastic modulus (E) = 1 Pa, density (ρ) = 1 kg/m^3, Poisson ratio (ν) = 0.3) and 300 × 50 Q4 elements (element size is 0.02 m). The left side of the beam is clamped and a harmonic force F = 1 N is applied in the bottom of the left size. The resulting frequency responses of 0 to 0.5 rad/s is shown in the Fig. 4 as a reference solution. Before the partial design problem, the conventional static compliance problem in the whole design domain ($\Omega^{(D)} = \Omega^{(1)} \cup \Omega^{(2)} \cup \Omega^{(3)}$) is considered. The static compliance is minimized to within 30% of the whole design domain volume. Figure 5 illustrates the optimization layout for the static compliance problem using both the conventional and proposed substructuring approaches. Note that the filtering radius is set to 1.5 times of the element length. Comparing Fig. 5a and b, a slight discrepancy in the optimization results under the same conditions becomes apparent, attributed to the numerical errors arising from the implementation of the substructuring approach. The relative error of sensitivity values in initial state (iter. = 1) is shown in Fig. 6a. On the other hand, Fig. 5c illustrates the variations in the optimal results when constraints are applied to each individual subdomain. Comparing Fig. 5c and d, it becomes evident that a more favorable topology can be achieved with refined mesh. Furthermore, as a reference of our computing hardware and software configurations, we have provided a summary of the elapsed time required to execute a single iteration of the optimization loop, as detailed in Table 2.

Now three different optimization approaches will be compared in the partial optimization problem: the conventional TO without any reduction scheme, the TO with conventional MR approach, and the proposed TO with substructuring approach. Considering clarity and simplicity for implementation of TO process, the MS and CB method are adopted as conventional MR and substructuring approach, respectively. For the MS and substructuring cases, 20 dominant structural and substructural modes are selected. Each subdomain in the Fig. 4 will be set as design domain once, while the remaining subdomains becomes non(passive)-design domains. In addition, the in Eq. (55) is adopted here with filtering radius $r_{\min} = 0.03$ (1.5 times of element length). The dynamic compliance in the low frequency interval ($\omega \in [0, 0.001]$ rad/s, $\Delta\omega = 0.001/NS, NS = 50$) is minimized to within 30% of the design domain volume (76% of the whole domain volume) to show similar layout of the design layout minimizing the static compliance as an reference result.

For the presented example with 15000 elements and 19803 DOFs takes about 5385.39 s, 821.45 s, 750.48 s in average, which shows effectiveness of the presented substructuring approach. Even the size of reduced matrix for the substructuring approach is much larger the size of reduced matrix for the conventional MR approach, less computation time is needed to reach optimization results because the conventional MR approach should solve eigenvalue problem at each iteration. These results demonstrate a notable advantage of presented substructuring approach. Figures 7 and 8 show the layout and frequency response function curves of the topology optimization with respect to the applied method. Both the full order model (FOM) and the conventional MR utilized passive design variable, $\boldsymbol{\gamma}^{(ND)} = 1$, resulting in almost the same optimization layout as shown in Fig. 7a and b. However, at the bottom result of Fig. 7b, the topology did not converge properly, and the FRF curve of the result could not be obtained (Fig. 8c).

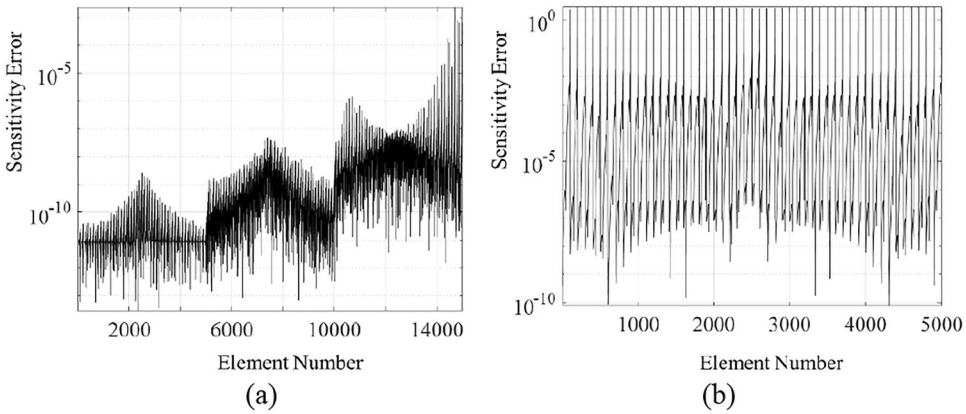

Fig. 6 Relative error of sensitivity values for each element. **a** Whole design domain case ($\Omega^{(D)} = \Omega^{(1)} \cup \Omega^{(2)} \cup \Omega^{(3)}$), **b** Partial design domain case ($\Omega^{(D)} = \Omega^{(1)}$)

Table 2 Main processes and computation times for topology optimization with respect to system size (A single repetition)

System Size Computation time (s)	1.32E+03	5.04E+03	1.21E+05	4.82E+05	3.01E+06	1.20E+07
Design variable update	0.0103	0.0143	0.2542	1.1361	6.2153	23.8362
System solve	0.0519	0.0610	1.0179	5.0801	43.2872	363.6840
Sensitivity calculation	0.0030	0.0018	0.0561	0.1177	0.4903	1.7265
MMA optimizer	0.0130	0.0982	0.6099	4.4339	18.4316	65.8600
Total	0.2339	0.3328	2.2523	11.5929	72.2597	470.0241

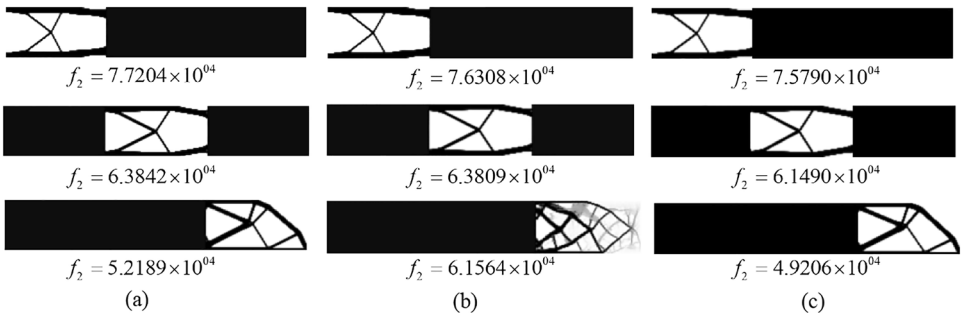

Fig. 7 Optimization results with **a** full order model (w/o reduction scheme), **b** conventional MR scheme (mode superposition method), **c**) presented substructuring scheme

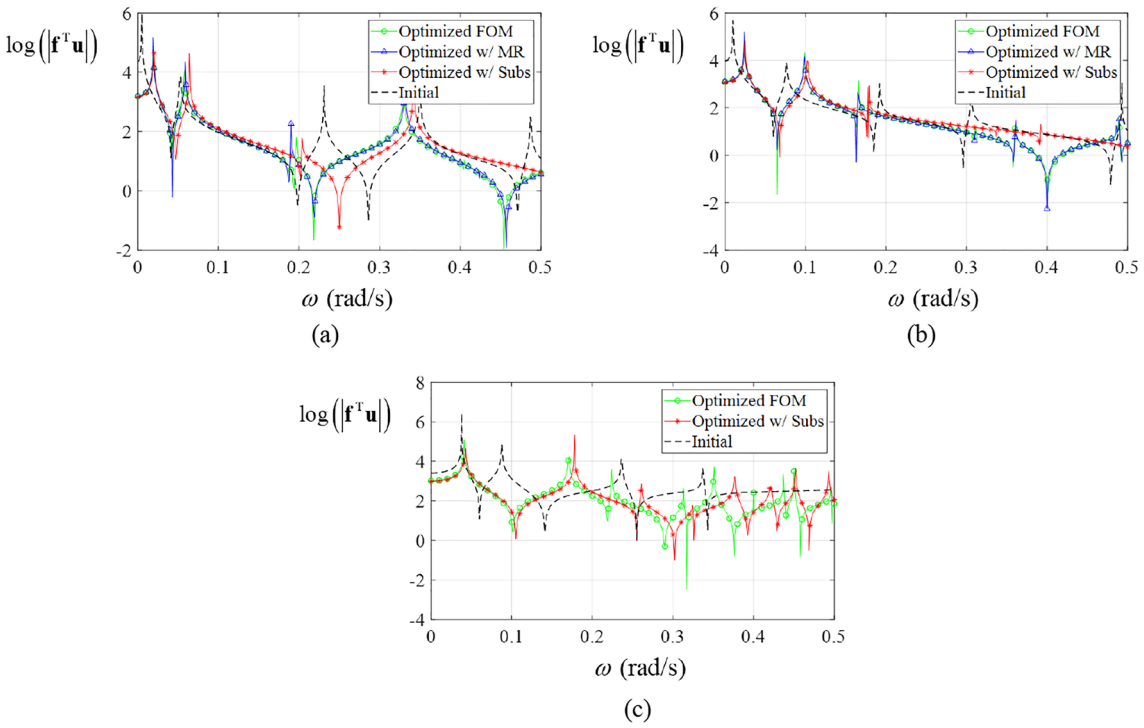

Fig. 8 Comparison of the frequency response curves of optimized design with respect to the FOM, MR, and substructuring methods for each design domain case; **a** $\Omega^{(D)} = \Omega^{(1)}$, **b** $\Omega^{(D)} = \Omega^{(2)}$, and **c** $\Omega^{(D)} = \Omega^{(3)}$

This issue arises from using localized modes, which are common in designs featuring significant density variations (known as "0–1" designs), during the model reduction process. It's a notable problem that occurs when applying mode-based order reduction to topology optimization. In addition, a noteworthy observation emerges: the disparity in the sensitivity values of elements with the interface DOF (relative errors are depicted in Fig. 5), does not significantly affect the optimal design outcome contrasting Fig. 7a and c.

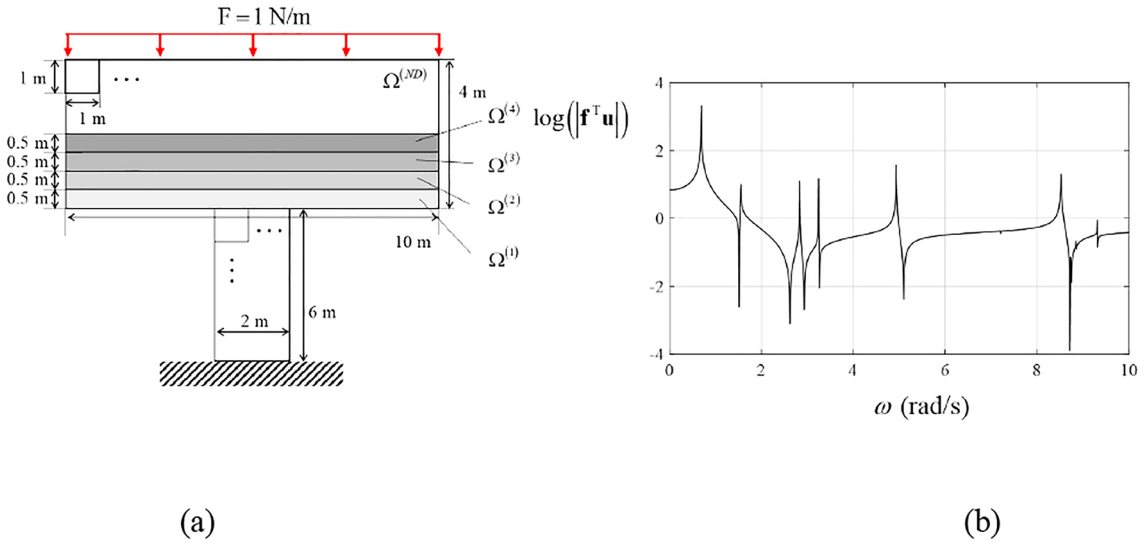

Fig. 9 Hammerhead pier design problem. **a** Problem definition with four different design layer ($E^{(1)} = 100$ Pa,$E^{(2)} = 200$ Pa,$E^{(3)} = 300$ Pa ,$E^{(4)} = 400$ Pa) and **b** compliance response curve to frequency

4.2 Hammerhead pier optimization

A hammerhead pier was chosen as the next example. This structure can model a massive bridge structure for which the consideration of harmonic resonance is required. The objective of this example is to design a center layer of the hammerhead pier considering gradually increasing structural stiffness. The top layer and the pier part are considered as non-design domains while the four supporting middle layers are optimized for minimum dynamic compliance subject to graded stiffness and harmonic distributed loads as depicted in Fig. 9a. In this example, the elastic moduli(E) for the non-design domain and four subdomains are set to be 100, 100, 200, 300, and 400 Pa from the bottom to the top, respectively. Other material properties are set to be same as the previous example (density (ρ) = 1 kg/m^3, Poisson ratio = 0.3) and the problem geometry is discretized with 0.005 m × 0.005 m Q4 elements. The dynamic compliance in the both low frequency domain ($\omega \in [0, 0.5]$ rad/s) and high frequency domain($\omega \in [1.25, 1.4]$ rad/s) with small number of frequency steps($\Delta\omega = \left(\omega_e - \omega_s\right)/NS, NS = 50$) will be minimized in this example. The frequency responses (compliance value at a specific frequency) and target frequency ranges for dynamic topology optimization problem can be found in Fig. 9b, Fig. 10a and d. An 1 m × 1 m repetitive geometry with same discretization is used to define the large-scale FE models in the non-design domains resulting in a FE model having 2,080,000 elements and 4,202,472 DOFs(Note that the total number of DOFs is calculated as the sum of the DOFs of each subdomain). And 10 dominant substructural modes are selected for the reduction of FE matrices in the non-design domains. Figure 10 shows the results of the example obtained by assigning the 30% volume constraint for each subdomain and implementing filter with $r_{\min} = 0.015$. As shown in Fig. 10c, optimized design in the low-frequency range shows that a fractal-like structure

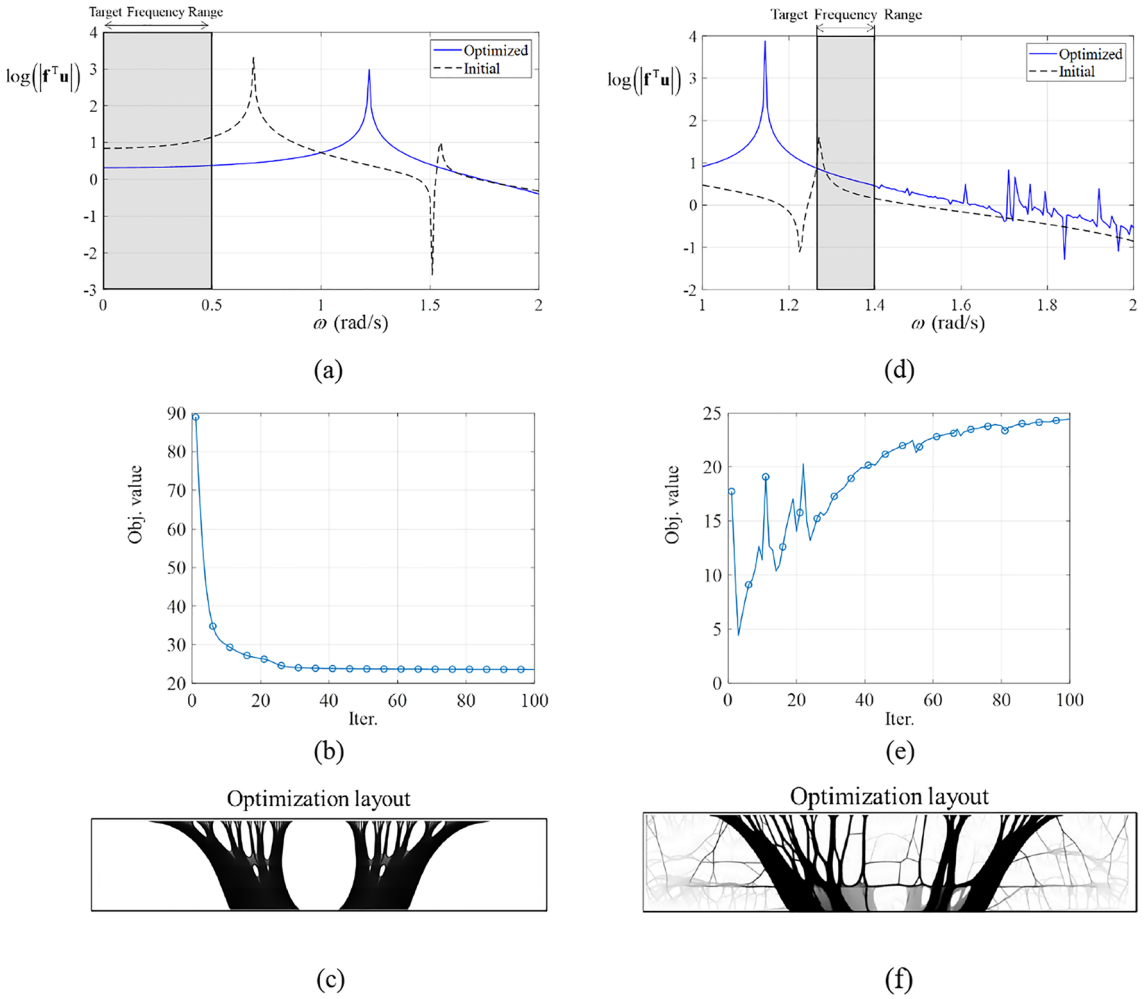

Fig. 10 Optimization results for hammerhead pier. **a** Compliance response curve to frequency, **b** objective function value history, **c** optimized layout in low-frequency domain ([0, 0.5](rad/s)). **d** Compliance response curve to frequency, **e** objective function value history, **f** optimized layout in high frequency domain ([1.25, 1.4](rad/s))

which easily can be found in nature structures in addition to a smooth transition between the subdomains.

Meanwhile optimized design in the high frequency range shows different appearance from that in the low frequency range. The most notable aspect of the optimization results in the high-frequency range is the increase in gray elements, a phenomenon frequently observed in other literature on topology optimization of dynamic systems or eigenvalue maximization problems (Yoon 2010; Zhao et al. 2018; Li et al. 2021). This increase often leads to some disconnection between the design subdomains. Mathematically, these gray elements arise due to the differences in penalty values for stiffness and mass. The typical penalty values ($p_k = 3$, $p_m = 1$) result in a very small stiffness when compared to mass. Consequently, these elements are much more flexible in comparison to areas with elements having full densities. They primarily affect the lowest eigenmodes (or resonant frequencies) of the entire structure, but do not influence the stiffness of the entire structure. In other words, the gray elements are not essential for preserving the overall structural rigidity, and therefore may not require a continuous connection to each other. The gray elements used to be interpreted as porous materials from an engineering perspective, but still designer may want a black/white design. Various finite element techniques have been investigated to eliminate the gray component. In this example, we opted for the two different approaches. One is putting higher penalty values on mass penalizing ($p_m = 6$). The other is utilizing the minimum density proposed by Tenek and Hagiwara(Tenek and Hagiwara 1994). A minimum density factor of 0.1 ($\gamma_{\min} = 0.1$) is chosen. Figure 11 shows the optimized design in the high frequency range with the higher penalty values and minimum density value. As shown in Fig. 11b, a higher mass penalty value may reduce the gray region but blurs the micro-topology of static results. Meanwhile, the gray background in Fig. 11d shows that the problem of a topology optimization has been replaced with an optimization of reinforcement. The optimized design in Fig. 11d become similar to the optimized design in the low frequency domain (Fig. 10c), with some reinforcing structures around the main fractal-like structure. Another noteworthy point is that the mode shifting during the dynamic optimization process causes an irregular increase in the objective function value, which can be seen through the objective function history curve in Fig. 9b and e (Note that the convergence criteria in Eq. (54) was not used to show the iteration history under same conditions).

4.3 Deep beam restoration and supporter optimization

An attempt to show the effectiveness of presented technique for design strengthening for engineering structures

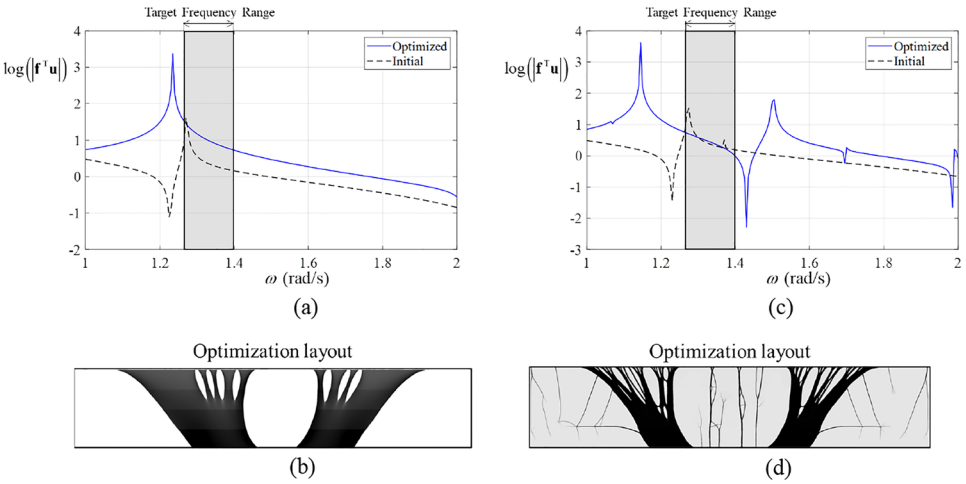

Fig. 11 Optimization results of hammerhead with higher mass penalty ($p_m = 6$) and minimum density ($\gamma_{\min} = 0.1$). **a** Compliance response curve to frequency and **b** optimized layout with higher mass penalty, **c** Compliance response curve to frequency and **d** optimized layout with minimum density

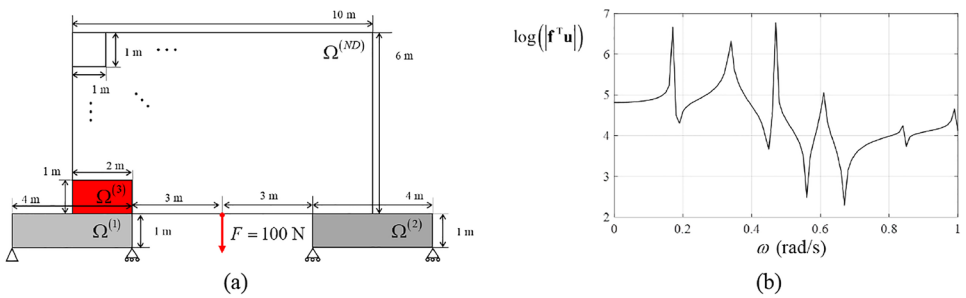

Fig. 12 Degraded deep beam marked in red and supporters. **a** Problem geometry and **b** compliance response curve to frequency

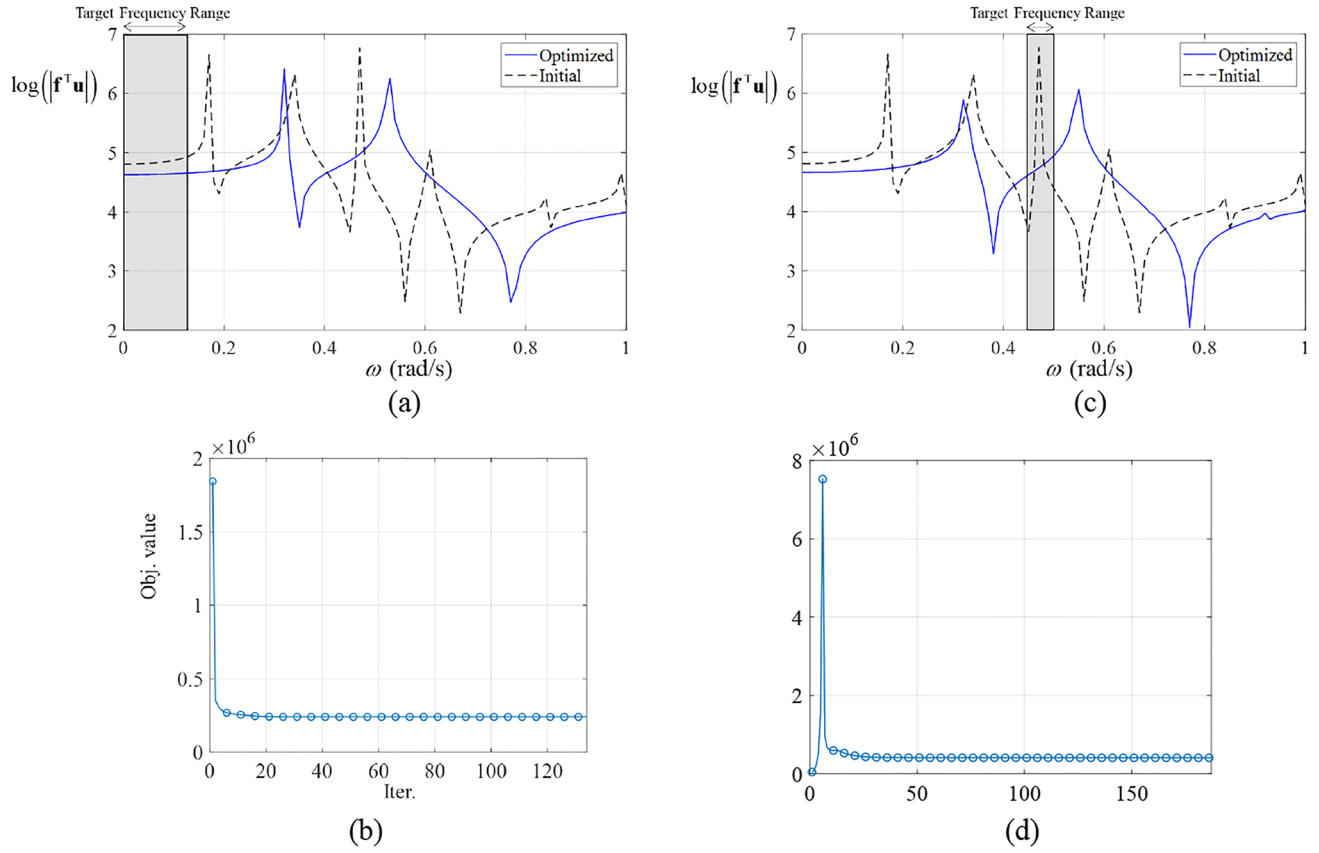

Fig. 13 Optimization results of degraded deem beam and supports. **a** Compliance response curve to frequency around the low target frequency ([0, 0.16](rad/s)), and **b** objective function value history. **c** Compliance response curve to frequency around the high target frequency ([0.48, 0.5](rad/s)), and **d** objective function value history

suffering from the effects of material degradation is made in this section. It is proposed to solve minimum compliance problem of asymmetric structure due to the material degradation and further restoration process for weakened substructures. Restoration process is conducted as a topology optimization task, in which the strengthening with a low volume of structural density (0.5) and maximal stiffness are sought for. As an example of strengthening, a deep beam with a concentrated force equal to $F = 100$ N and supporter are presented as shown in Fig. 12. The material properties for the supporting structure are set to $E = 1000$ Pa,$\rho = 1$ kg/m^3,$\nu = 0.3$, and those for the deep deem are set to $E = 10$ Pa,$\rho = 1$ kg/m^3,$\nu = 0.3$. The problem is discretized with 0.002 m $\times$ 0.002 m Q4 elements yielding 17,000,000 elements and 34,130,124 DOFs and a 1 m $\times$ 1 m repetitive geometry with same discretization, and 10 dominant substructural modes are selected for the reduction of the non-design domains. Lastly, the filter radius is set to $r_{\min} = 0.004$.

Figure 13 shows the optimization results of the example with volume constraint of 0.4 for the supporter structures ($\Omega^{(1)}, \Omega^{(2)}$) and 0.5 for the degraded substructure ($\Omega^{(3)}$). In this optimization problem, it took 134 and 187 iterations to satisfy the convergence criteria in Eq. (54) for problems in the low [0 0.16](rad/s) and high [0.48 0.5](rad/s) target frequency range. Figure 13b and d show the iterations history of each problem. Figure 14a and b show a smooth transition of the material between the substructures that would be difficult to achieve if the filtering was performed separately.

In addition, the results in Figs. 13d and 14b, a monotonic convergence of objective function value and fewer gray elements in optimization layout result, denote that resonant frequency shift or instability phenomenon during the topology optimization in high-frequency range causes gray elements in the optimal layout and this phenomenon does not always happen.

5 Conclusions

This study introduces a new dynamic topology optimization process that uses a substructuring approach for large-scale systems in the frequency domain. The method

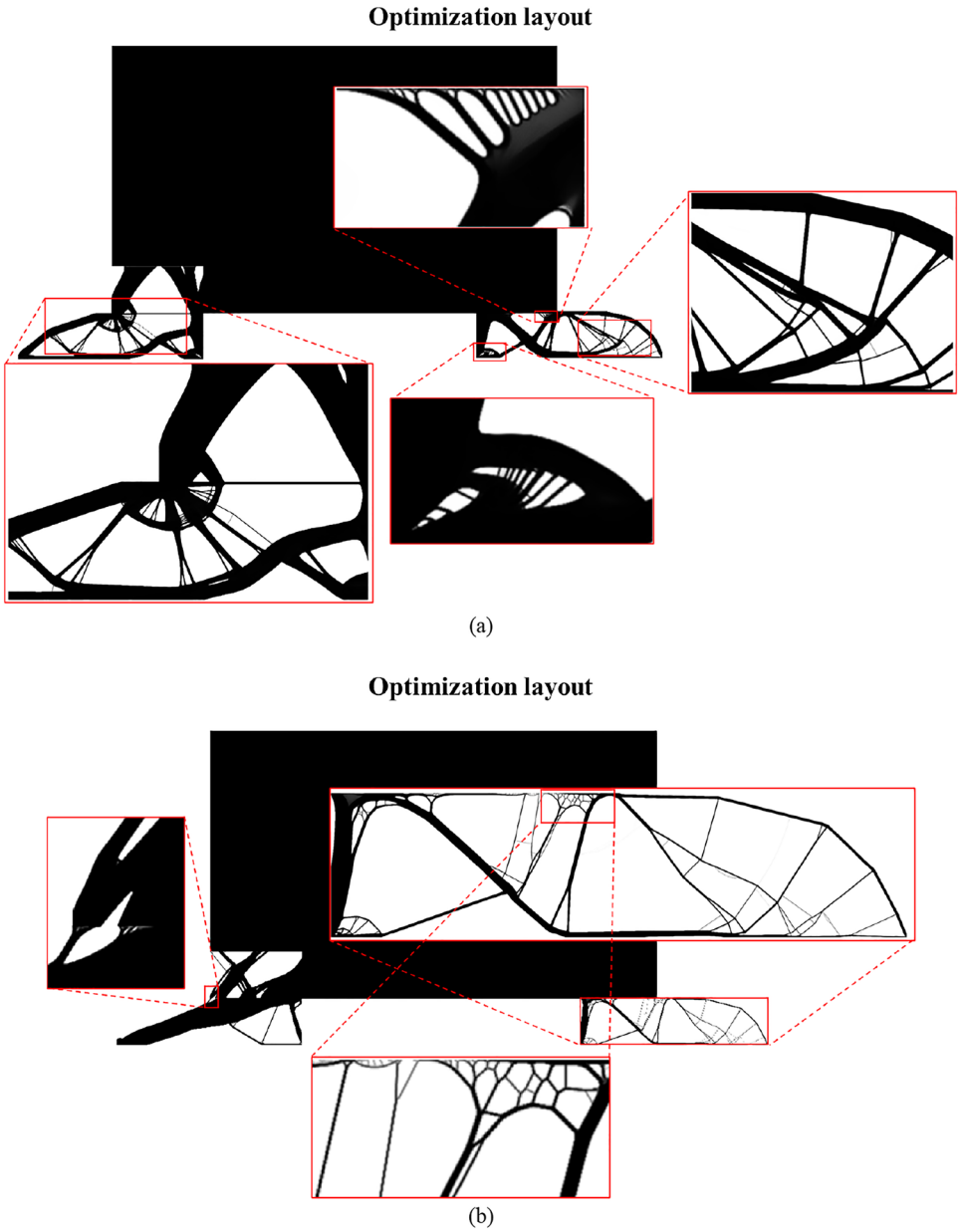

Fig. 14 Optimization results of degraded deem beam and supports. **a** Optimized layout in low frequency domain ([0, 0.16](rad/s)), and **b** in high-frequency domain([0.48, 0.5] (rad/s))

enables solving large-scale topology optimization problems in a more practical and realistic manner, taking into account the simultaneous design of multi-component structures, composed of different materials, and with different constraints. The traditional optimal design problem requires determining the response of the entire system, even if only a part of the system needs to be optimized, which can be challenging for complex and large-scale structures. Solving a frequency domain system necessitates iterative inverse operations, and frequency-dependent matrix conditions make it challenging to use pcg solvers and their preconditioners, which are typically used to solve large-scale problems. To solve this issue, this paper introduces a partial topology optimization technique that utilizes two fundamental principles: (1) substructuring approach and (2) repetitive geometry. The nodal variables related to the non-design domains are segmented and removed by repetitive geometry, and finally approximated by the substructuring technique (Although we employ the basic Craig–Brampton method here, the presented optimization process can utilize any kind of dynamic substructuring method). Thereby presented partial TO process allows the designer to deal with much larger systems by only handling the nodal variables related to the design domains as well as different objectives and constraints among the

different design subdomains at the same time. Several topology optimization examples have been presented to demonstrate the performance of the proposed method in large-scale topology optimization problems.

Author contributions HSK and GHY: Conceptualization and methodology. HSK: Investigation and writing. GHY: Review. GHY: Funding acquisition and supervision.

Funding This work was supported by the National Research Foundation of Korea (NRF) grant funded by the Korea government (MSIT) (No.2018R1A5A7025522).

Data availability Not applicable.

Code availability Not applicable.

Declarations

Conflict of interest On behalf of all authors, the corresponding author states that there is no conflict of interest.

Replication of results The presented results were mainly obtained using our MATLAB codes and may be provided on reasonable request.

References

Aage N, Lazarov BS (2013) Parallel framework for topology optimization using the method of moving asymptotes. Struct Multidisc Optim 47:493–505

Aage N, Andreassen E, Lazarov BS (2015) Topology optimization using PETSc: an easy-to-use, fully parallel, open source topology optimization framework. Struct Multidisc Optim 51:565–572

Aage N, Andreassen E, Lazarov BS, Sigmund O (2017) Giga-voxel computational morphogenesis for structural design. Nature 550:84–86

Alexandersen J, Sigmund O, Aage N (2016) Large scale three-dimensional topology optimisation of heat sinks cooled by natural convection. Int J Heat Mass Transf 100:876–891

Amir O (2015) Revisiting approximate reanalysis in topology optimization: on the advantages of recycled preconditioning in a minimum weight procedure. Struct Multidisc Optim 51:41–57

Amir O, Sigmund O (2011) On reducing computational effort in topology optimization: how far can we go? Struct Multidisc Optim 44:25–29

Amir O, Stolpe M, Sigmund O (2010) Efficient use of iterative solvers in nested topology optimization. Struct Multidisc Optim 42:55–72

Bathe K-J (2006) Finite element procedures: Klaus-Jurgen Bathe.

Bendsøe MP, Kikuchi N (1988) Generating optimal topologies in structural design using a homogenization method. Comput Methods Appl Mech Eng 71:197–224

Botkin ME, Yang RJ (1991) Three-dimensional shape optimization with substructuring. AIAA J 29:486–488

Carlberg K, Forstall V, Tuminaro R (2016) Krylov-subspace recycling via the POD-augmented conjugate-gradient method. SIAM J Matrix Anal Appl 37:1304–1336

Choi Y, Oxberry GM, White D, Kirchdoerfer T (2019) Accelerating design optimization using reduced order models. ArXiv abs/1909.11320.

Cornwell RE, Craig RR Jr, Johnson CP (1983) On the application of the mode-acceleration method to structural engineering problems. Earthquake Eng Struct Dynam 11:679–688

Craig RR, Bampton MCC (1968) Coupling of substructures for dynamic analyses. AIAA J 6:1313–1319

de Klerk D, Rixen DJ, Voormeeren SN (2008) General framework for dynamic substructuring: history, review and classification of techniques. AIAA J 46:1169–1181

Evgrafov A, Rupp CJ, Maute K, Dunn ML (2008) Large-scale parallel topology optimization using a dual-primal substructuring solver. Struct Multidisc Optim 36:329–345

Farhat C, Roux F-X (1991) A method of finite element tearing and interconnecting and its parallel solution algorithm. Int J Numer Meth Eng 32:1205–1227

Hurty Walter C (1960) Vibrations of structural systems by component mode synthesis. J Eng Mech Div 86:51–69

Irons B (1965) Structural eigenvalue problems - elimination of unwanted variables. AIAA J 3:961–962

Jensen JS (2007) Topology optimization of dynamics problems with Padé approximants. Int J Numer Meth Eng 72:1605–1630

Kang Z, He J, Shi L, Miao Z (2020) A method using successive iteration of analysis and design for large-scale topology optimization considering eigenfrequencies. Comput Methods Appl Mech Eng 362:112847

Kikuchi N, Nishiwaki S, Fonseca JSO, Silva ECN (1998) Design optimization method for compliant mechanisms and material microstructure. Comput Methods Appl Mech Eng 151:401–417

Kim TS, Kim JE, Kim YY (2004) Parallelized structural topology optimization for eigenvalue problems. Int J Solids Struct 41:2623–2641

Koh HS, Kim JH, Yoon GH (2020) Efficient topology optimization of multicomponent structure using substructuring-based model order reduction method. Comput Struct 228:106146

Kristiansen H, Aage N (2022) An open-source framework for large-scale transient topology optimization using PETSc. Struct Multidisc Optim 65:295

Le C, Norato J, Bruns T, Ha C, Tortorelli D (2010) Stress-based topology optimization for continua. Struct Multidisc Optim 41:605–620

Li Q, Sigmund O, Jensen JS, Aage N (2021) Reduced-order methods for dynamic problems in topology optimization: a comparative study. Comput Methods Appl Mech Eng 387:114149

Liu H, Zhang W, Gao T (2015) A comparative study of dynamic analysis methods for structural topology optimization under harmonic force excitations. Struct Multidisc Optim 51:1321–1333

Ma ZD, Kikuchi N, Hagiwara I (1993) Structural topology and shape optimization for a frequency response problem. Comput Mech 13:157–174

Ma Z-D, Cheng H-C, Kikuchi N (1994) Structural design for obtaining desired eigenfrequencies by using the topology and shape optimization method. Comput Syst Eng 5:77–89

Ma Z-D, Kikuchi N, Cheng H-C (1995) Topological design for vibrating structures. Comput Methods Appl Mech Eng 121:259–280

Ma Z-D, Kikuchi N, Pierre C, Raju B (2005) Multidomain topology optimization for structural and material designs. J Appl Mech 73:565–573

MacNeal RH (1971) A hybrid method of component mode synthesis. Comput Struct 1:581–601

Mahdavi A, Balaji R, Frecker M, Mockensturm EM (2006) Topology optimization of 2D continua for minimum compliance using parallel computing. Struct Multidisc Optim 32:121–132

Nishiwaki S, Frecker MI, Min S, Kikuchi N (1998) Topology optimization of compliant mechanisms using the homogenization method. Int J Numer Meth Eng 42:535–559

Noor AK, Kamel HA, Fulton RE (1978) Substructuring techniques—status and projections. Comput Struct 8:621–632

Pedersen NL (2000) Maximization of eigenvalues using topology optimization. Struct Multidisc Optim 20:2–11
Rubin S (1975) Improved component-mode representation for structural dynamic analysis. AIAA J 13:995–1006
Schmidt S, Schulz V (2011) A 2589 line topology optimization code written for the graphics card. Comput vis Sci 14:249–256
Sigmund O (2001) A 99 line topology optimization code written in Matlab. Struct Multidisc Optim 21:120–127
Stewart GW (2002) A Krylov-Schur algorithm for large eigenproblems. SIAM J Matrix Anal Appl 23:601–614
Tenek HL, Hagiwara I (1994) Eigenfrequency maximization of plates by optimization of topology using homogenization and mathematical programming. JSME Int J Ser c, Dynam, Control, Robot, Des Manuf 37:667–677
Träff EA, Sigmund O, Aage N (2021) Topology optimization of ultra high resolution shell structures. Thin-Walled Struct 160:107349
Vemaganti K, Lawrence WE (2005) Parallel methods for optimality criteria-based topology optimization. Comput Methods Appl Mech Eng 194:3637–3667
Wadbro E, Berggren M (2009) Megapixel topology optimization on a graphics processing unit. SIAM Rev 51:707–721
Wang S, Sturler Ed, Paulino GH (2007) Large-scale topology optimization using preconditioned Krylov subspace methods with recycling. International Journal for Numerical Methods in Engineering. 69: 2441–2468.
Wilson EL (1974) The static condensation algorithm. Int J Numer Meth Eng 8:198–203
Wu Z, Xia L, Wang S, Shi T (2019) Topology optimization of hierarchical lattice structures with substructuring. Comput Methods Appl Mech Eng 345:602–617
Yang RJ, Chen CJ (1996) Stress-Based Topology Optimization. Struct Optimiz 12:98–105
Yoon GH (2010) Structural topology optimization for frequency response problem using model reduction schemes. Comput Methods Appl Mech Eng 199:1744–1763
Yoon GH (2014) Stress-based topology optimization method for steady-state fluid–structure interaction problems. Comput Methods Appl Mech Eng 278:499–523
Zhang W, Sun S (2006) Scale-related topology optimization of cellular materials and structures. Int J Numer Meth Eng 68:993–1011
Zhao X, Wu B, Li Z, Zhong H (2018) A method for topology optimization of structures under harmonic excitations. Struct Multidisc Optim 58:475–487